Circular RNA Vaccines against SARS-CoV-2 and Emerging Variants

Liang Qu[1]*, Zongyi Yi[1,2]*, Yong Shen[1,2], Yiyuan Xu[1], Zeguang Wu[1], Huixian Tang[1], Xia Xiao[3], Xiaojing Dong[3], Li Guo[3], Ayijiang Yisimayi[4], Yunlong Cao[4], Zhuo Zhou[1], Jianwei Wang[3], Xiaoliang Sunney Xie[4], Wensheng Wei[1]†

[1]Biomedical Pioneering Innovation Center, Beijing Advanced Innovation Center for Genomics, Peking-Tsinghua Center for Life Sciences, Peking University Genome Editing Research Center, State Key Laboratory of Protein and Plant Gene Research, School of Life Sciences, Peking University, Beijing 100871, China. [2]Academy for Advanced Interdisciplinary Studies, Peking University, Beijing 100871, China. [3]NHC Key Laboratory of Systems Biology of Pathogens and Christophe Mérieux Laboratory, Institute of Pathogen Biology, Chinese Academy of Medical Sciences and Peking Union Medical College, Beijing 100730, China; Key Laboratory of Respiratory Disease Pathogenomics, Chinese Academy of Medical Sciences and Peking Union Medical College, Beijing 100730, China. [4]Biomedical Pioneering Innovation Center, Beijing Advanced Innovation Center for Genomics, Peking-Tsinghua Center for Life Sciences, Peking University, Beijing 100871, China.

*These authors contributed equally to this work.

†Email: wswei@pku.edu.cn (W.W.)

Abstract: SARS-CoV-2 has caused a worldwide pandemic. The emerging variants B.1.1.7 in the UK, B.1.351 in South Africa, and P.1 in Brazil have recently spread rapidly, arousing concerns about the efficacy of the current vaccines and antibody therapies. Therefore, there is still a high demand for alternative vaccines with great efficacy, high design flexibility, and fast manufacturing speed. Here, we reported a circular RNA (circRNA) vaccine that encodes the trimeric RBD of SARS-CoV-2 spike protein. Being a circularized RNA molecule, circRNA^{RBD} could be rapidly produced via *in vitro* transcription and is highly stable without nucleotide modification. Lipid-nanoparticle-encapsulated circRNA^{RBD} elicited potent and sustained neutralizing antibodies, as well as Th1-biased T cell responses in mice. Notably, antibodies from mice immunized with circRNA encoding RBD variant (K417N-E484K-501Y) effectively neutralized B.1.351 variant.

Moreover, we developed therapeutic circRNAs, encoding SARS-CoV-2 neutralizing nanobodies or hACE2 decoys, which could effectively neutralize SARS-CoV-2 pseudovirus. Our study suggests that circular RNA holds the potential to become a novel vaccine and therapeutic platform.

Main Text:

Coronavirus disease 2019 (COVID-19) is a serious worldwide public health emergency caused by a novel severe acute respiratory syndrome coronavirus (SARS-CoV-2) (*1, 2*). To date, COVID-19 has resulted in more than one hundred million confirmed cases and over two million confirmed deaths (World Health Organization). Thus, there is an urgent need for the development of safe and effective vaccines against SARS-CoV-2 infection.

SARS-CoV-2, together with Severe Acute Respiratory Syndrome (SARS)-CoV and Middle East Respiratory Syndrome (MERS)-CoV, other two highly pathogenic coronaviruses, belongs to the genus *Betacoronavirus* of the *Coronaviridae* family (*3*). SARS-CoV-2 is a single-strand, positive-sense, enveloped virus, and its virion is composed of an inner capsid formed by 30-kb RNA genome wrapped by the nucleocapsid (N) proteins and a lipid envelope coated with the membrane (M), envelope (E), and trimeric spike (S) proteins (*4*). The S protein of SARS-CoV-2, composed of S1 and S2 subunits, is the major surface protein of the virion. The S protein mediates viral entry into host cells by binding to its receptor, angiotensin-converting enzyme 2 (ACE2), through the receptor-binding domain (RBD) at the C terminus of the S1 subunit. This binding subsequently induces the fusion between the SARS-CoV-2 envelope and the host cell membrane mediated by the S2 subunit, leading to the release of the viral genome into the cytoplasm (*5-8*).

The S protein, S1 subunit, or the RBD antigen of SARS-CoV-2, could induce both B cell and T cell responses, generating highly potent neutralizing antibodies against SARS-CoV-2 (*9-11*). Vaccination is the most promising approach to end COVID-19 pandemic. Traditional vaccine platforms, such as inactivated vaccines, virus-like particle vaccines, and viral vector-based vaccines have been adopted to develop SARS-CoV-2 vaccines (*12-20*). Importantly, the mRNA vaccines against SARS-CoV-2 have been developed at warp speed and urgently approved for use (*21-27*), despite the fact that such strategy had never been applied commercially before (*28*). The mRNA vaccine contains a linear single-strand RNA, consisting of 5' cap, the untranslated region (UTR), antigen-coding region, and 3' polyA tail, which is delivered into bodies via lipid-nano

60 particle (LNP) encapsulation (*28*). The clinical-scale mRNA vaccines could be manufactured
61 rapidly upon the viral antigen sequence is released (*21*). However, the current mRNA vaccine still
62 has certain limitations due to its inherent instability and suboptimal thermostability after LNP
63 encapsulation for *in vivo* administration (*29-31*), as well as potential immunogenic side effects (*32,*
64 *33*).

65 Circular RNAs (circRNAs) are covalently closed single-stranded RNA transcripts, comprising
66 a large class of non-coding RNAs generated by a non-canonical RNA splicing event called
67 backsplicing in eukaryotic cells (*34-36*). Some viral genomes happen to be circular RNAs, such as
68 hepatitis D virus and plant viroids (*33*). In recent years, thousands of circRNAs have been
69 identified in eukaryotes, including fungi, plants, insects, fish, and mammals via high-throughput
70 RNA sequencing and circRNA-specific bioinformatics (*36*). Unlike linear mRNA, circRNA is
71 highly stable as its covalently closed ring structure protects it from exonuclease-mediated
72 degradation (*36-38*). So far, only a few endogenous circRNAs have been shown to function as
73 protein translation templates (*39-42*). Although circRNA lacks the essential elements for cap-
74 dependent translation, it can be engineered to enable protein translation through internal ribosome
75 entry site (IRES) or the m6A modification incorporated to its 5' UTR region (*43, 44*).

76 Here, we developed circRNA vaccines against the native SARS-CoV-2 or its emerging
77 variants, which induced robust neutralizing antibodies and strong T cell responses in mice.
78 Moreover, circRNA could be employed to express nanobodies or AEC2 decoys to neutralize the
79 SARS-CoV-2 pseudovirus, manifesting its therapeutics potential to directly blockade such deadly
80 infections.

81

82 ***In Vitro* circRNA production by Group I ribozyme autocatalysis**

83 We adopted a Group I ribozyme autocatalysis strategy (*43*) to produce circular RNA encoding
84 SARS-CoV-2 RBD antigens (*23*), termed circRNA^{RBD} (Fig. 1A). To enhance the immunogenicity
85 of RBD antigens, we added a signal peptide sequence (SP) to the N-terminus of RBD for its
86 secretory expression (*45-47*). In this construct, the IRES element was placed before the RBD-
87 coding sequence to initiate its translation. The signal peptide sequence of human tissue
88 plasminogen activator (tPA) (*17, 45*) was fused to the N-terminus of RBD to ensure the secretion
89 of antigens, and the trimerization motif of bacteriophage T4 fibritin protein (foldon) (*48*) was fused

90 to its C terminus, mimicking the natural conformation of SARS-CoV-2 Spike trimers, which have
91 a superior hACE2 binding capacity to the monomeric RBD counterparts (*6, 7, 49*). This IRES-SP-
92 RBD-T4 sequence was then inserted into the cyclization vector (Fig. 1A) to generate the template
93 for *in vitro* transcription (IVT) in order to produce circRNA^{RBD}. The circularization of circRNA^{RBD}
94 was verified (Fig. 1B) by reverse transcription and RT-PCR analysis using specific primers (Fig.
95 1A).

96 Owing to this covalently closed circular structure, the circRNA^{RBD} migrated faster in
97 electrophoresis (fig. S1A) and appeared more resistant to exonuclease RNase R than the linear
98 RNAs (fig. S1B). Moreover, the high-performance liquid chromatography (HPLC) purification
99 showed that the RNase R treatment purged significant amount of the linear precursor RNAs, an
100 important step for the production and purification of the circRNA^{RBD} (fig. S1C).

101

102 **Thermal stable circRNA^{RBD} produces functional SARS-CoV-2 RBD antigens**

103 To test the secretory expression of RBD produced by circRNA^{RBD}, the purified circRNA^{RBD} was
104 transfected into HEK293T cells. We detected ample production of SARS-CoV-2 RBD antigens in
105 the supernatant by Western blot (Fig. 1C). Quantitative ELISA assay showed that the RBD protein
106 reached ~143 ng/mL in the supernatant, 50-fold more than the linear RNA^{RBD} group (Fig. 1D). We
107 further confirmed that circRNA^{RBD} could be expressed in murine NIH3T3 cells (Fig. 1E). Together,
108 these results demonstrated that robust secretory RBD antigens could be produced using
109 circRNA^{RBD} in both human and murine cells.

110 The inherent stability of circRNA has been reported (*50*), and such a feature would make
111 circRNA an attractive vaccine candidate. To test this, circRNA^{RBD} was stored at room temperature
112 (~25°C) for various days before transfected into HEK293T cells. We found that circRNA^{RBD} could
113 be readily expressed without detectable loss even after two weeks of shelf time (Fig. 1F),
114 highlighting its remarkable thermal stability.

115 To further verify whether the secreted SARS-CoV-2 RBD antigens produced by circRNA^{RBD}
116 were functional, the supernatants of circRNA^{RBD}-transfected cells were used for competition assay
117 using hACE2-overexpressing HEK293 cells (HEK293T-ACE2) and SARS-CoV-2 pseudovirus
118 harboring an EGFP reporter (*51*). We witnessed that the secreted SARS-CoV-2 RBD antigens

119 could effectively block SARS-CoV-2 pseudovirus infection (Fig. 1G and fig. S2). Altogether,
120 circRNA^{RBD} showed robust protein expression and high thermal stability, illuminating its potential
121 for vaccination.

122

123 **SARS-CoV-2 circRNA vaccines elicit sustained humoral immune responses with high-level**
124 **neutralizing antibodies**

125 With its stability and immunogen-coding capability, we reasoned that circRNA could be developed
126 into a new type of vaccine. We then attempted to assess the immunogenicity of circRNA^{RBD}
127 encapsulated with lipid nanoparticle in BALB/c mice (Fig. 2A). The circRNA^{RBD} encapsulation
128 efficiency was greater than 93%, with an average size of 100 nm in diameter (Fig. 2B). Animals
129 were immunized with LNP-circRNA^{RBD} through intramuscular injection twice, using a dose of 10
130 μg or 50 μg per mouse at a two-week interval, while empty LNP was used as the placebo (Fig.
131 2C). The amount of RBD-specific IgG and pseudovirus neutralization activity were evaluated at
132 two or five weeks post LNP-circRNA^{RBD} boost.

133 High titers of RBD-specific IgG were elicited by circRNA^{RBD} in a dose-dependent manner,
134 ~3×10^4 and ~1×10^6 for each dose and for both 2- and 5-weeks post boost, indicating that
135 circRNA^{RBD} could induce long-lasting antibodies against SARS-CoV-2 RBD (Fig. 2D).

136 To test the antigen-specific binding capability of IgG from vaccinated animals, we performed a
137 surrogate neutralization assay (*52*). In line with the amount of RBD-specific IgG (Fig. 2D),
138 antibodies elicited by circRNA^{RBD} vaccines showed evident neutralizing capacity in dose-
139 dependent manner, with an NT50 of ~2×10^4 for the dose of 50 μg (Fig. 2, E and F).

140 We further demonstrated that sera from circRNA^{RBD}-vaccinated mice neutralized SARS-CoV-
141 2 pseudovirus (Fig. 2G), with an NT50 of ~5.6×10^3 in mice immunized with 50 μg of circRNA^{RBD}
142 vaccine. The large amount of RBD-specific IgG, potent RBD antigen neutralization, and sustained
143 SARS-CoV-2 pseudovirus neutralizing capacity suggest that circRNA^{RBD} vaccines did induce a
144 long-lasting humoral immune response in mice.

145

146 **SARS-CoV-2 circRNA vaccines induce strong T cell immune responses in the spleen**

147 B cells (the source of antibodies), CD4$^+$ T cells, and CD8$^+$ T cells are three pillars of adaptive

148 immunity, and they mediated effector functions that have been associated with the control of
149 SARS-CoV-2 in both non-hospitalized and hospitalized cases of COVID-19 (*53*).

150 To probe $CD4^+$ and $CD8^+$ T cell immune responses in $circRNA^{RBD}$ vaccinated mice (5 weeks
151 post-boost), splenocytes were stimulated with SARS-CoV-2 Spike RBD pooled peptides (Table
152 S1), and cytokine-producing T cells were quantified by intracellular cytokine staining among
153 effector memory T cells (Tem, $CD44^+CD62L^-$) (fig. S3). Stimulated with RBD peptide pools,
154 $CD4^+$ T cells of mice immunized with $circRNA^{RBD}$ vaccines exhibited Th1-biased responses,
155 producing interferon-γ (IFN-γ), tumor necrosis factor (TNF-α), and interleukin-2 (IL-2) (Fig. 3, A
156 and B), but not interleukin-4 (IL-4) (fig. S4), indicating that $circRNA^{RBD}$ vaccines mainly induced
157 the Th1- but not the Th2-biased immune responses. In addition, multiple cytokine-producing $CD8^+$
158 were detected in $circRNA^{RBD}$ vaccinated mice (Fig. 3, C and D). For unknown reasons, 10 μg of
159 $circRNA^{RBD}$ elicited stronger immune responses in both $CD4^+$ and $CD8^+$ effector memory T cells
160 than 50 μg (Fig. 3, A to D), while the latter induced higher potency of neutralizing antibodies in
161 the B cell responses (Fig. 2G).

162 Collectively, these results demonstrated that SARS-CoV-2 $circRNA^{RBD}$ vaccines could induce
163 high level of humoral and cellular immune responses in mice.

164

165 **SARS-CoV-2 $circRNA^{RBD\text{-}501Y.V2}$ vaccines show preferential neutralization activity against**
166 **B.1.351 variant**

167 Next, we evaluated the efficacy of a circRNA vaccine encoding RBD/K417N-E484K-N501Y
168 derived from the B.1.351/501Y.V2 variant, termed as $circRNA^{RBD\text{-}501Y.V2}$ (Fig. 4A). BALB/c mice
169 were immunized with an i.m. injection of the $circRNA^{RBD\text{-}501Y.V2}$ vaccine, followed by a boost at a
170 two-week interval. The immunized mice's sera were collected at 1 and 2 weeks post the boost. The
171 ELISA showed that the RBD-501Y.V2-specific IgG titer reached 7×10^4 at 2 weeks post boost (Fig.
172 4B). The surrogate neutralization assay showed that sera of $circRNA^{RBD\text{-}501Y.V2}$ immunized mice
173 effectively neutralized RBD antigens (Fig. 4C). We then went on to assess the neutralization
174 activity of the sera from mice immunized with $circRNA^{RBD}$ or $circRNA^{RBD\text{-}501Y.V2}$ vaccines against
175 D614G, B.1.1.7/501Y.V1, or B.1.351/501Y.V2 variants. VSV-based pseudovirus neutralization
176 assay revealed that antibodies elicited by $circRNA^{RBD}$ vaccines, which encode the native RBD
177 sequence, effectively neutralized all three viral strains, with the highest activity against the D614G

178 strain (Fig. 4D). The circRNA$^{RBD\text{-}501Y.V2}$ immunized mouse serum could also neutralize all three
179 pseudoviruses, with the highest neutralization activity against its corresponding variant, 501Y.V2
180 (Fig. 4E). Collectively, circRNA vaccines-elicited antibodies showed the best neutralization
181 activity against their corresponding variant strains. It's worth noting that both vaccines could
182 neutralize all three strains albeit with variable efficacies. Nevertheless, the multivalent vaccines
183 should have provided better protection for both native SARS-CoV-2 strain and its circulating
184 variants.

185

186 **Expression of SARS-CoV-2 neutralizing antibodies via circRNA platform**

187 Besides vaccine, circRNA could be re-purposed for therapeutics when used to express some other
188 proteins or peptides, such as enzymes for rare diseases and antibodies for infectious diseases or
189 cancer. Here, we attempted to test the therapeutic potential of circRNAs by expressing the SARS-
190 CoV-2 neutralizing antibodies. It has been reported that SARS-CoV-2 neutralizing nanobodies or
191 hACE2 decoys could inhibit the SARS-CoV-2 infection (*54-56*). This prompted us to leverage the
192 circRNA platform to express SARS-CoV-2 neutralizing nanobodies, including nAB1, nAB1-Tri,
193 nAB2, nAB2-Tri, nAB3, and nAB3-Tri (*54, 55*), together with hACE2 decoys (*56*) (Fig. 5A).
194 Pseudovirus neutralizing assay showed that supernatants of HEK293T cells transfected with
195 circRNA^{nAB} or circRNA$^{hACE2\ decoys}$ could effectively inhibit pseudovirus infection (Fig. 5B).
196 Among those, nAB1-Tri, nAB2, nAB2-Tri, and nAB3-Tri nanobodies produced by circRNAs
197 completely blocked pseudovirus infection.

198

199 **Discussion**

200 COVID-19 is still a fast-growing global health crisis with circulating SAS-CoV-2 variants evading
201 current vaccines elicited antibodies (*57-59*). This report established a novel approach using
202 circRNA to produce SARS-CoV-2 related interventions, including vaccine, therapeutic
203 nanobodies, and hACE2 decoys.

204 Several studies have reported that the full-length Spike protein (mRNA-1273 and BNT162b2)
205 (*21, 22, 27*) or RBD-based mRNA vaccines elicit neutralizing antibodies and cellular immune
206 responses (*23-26, 60*). As reported, most effective neutralizing antibodies recognize the RBD

207 region of S protein (*54, 55, 61-64*) and targeting RBD may induce less amount of non-neutralizing
208 antibodies (*23-26, 60*). Given that RBD trimers were superior in binding hACE2 compared to their
209 monomeric counterparts (*49*), we chose to express RBD trimers as the immunogen.

210 We highlight this generalizable strategy for designing immunogens. The coding sequence of
211 circular RNA can be quickly adapted to deal with any emerging SARS-CoV-2 variants, such as
212 the recently reported B.1.1.7/501Y.V1, B.1.351/501Y.V2, and P.1 variants (*58, 65, 66*). Moreover,
213 circular RNAs could be quickly generated in large quantities *in vitro*, and they do not require any
214 nucleotide modification, strikingly different from the canonical mRNA vaccines. Interestingly,
215 circular RNA itself could serve as a vaccine adjuvant (*33*), suggesting that circRNA vaccine is
216 likely benefit from its own adjuvant effect.

217 In this report, circRNA$^{\text{RBD-501Y.V2}}$ immunized mice produced high titers of neutralizing
218 antibodies. Given that K417N-E484K-N501Y mutant in RBD reduces its interactions with certain
219 neutralizing antibodies (*58, 67*), we also demonstrated that neutralizing antibodies produced by
220 mice immunized with circRNA^{RBD} or circRNA$^{\text{RBD-501Y.V2}}$ had preferential neutralizing abilities to
221 their corresponding virus strains.

222 Multiple candidates for the treatment of COVID-19 have been studied during the pandemic,
223 especially those neutralizing antibodies (*54, 55, 61-64*) and engineered soluble natural receptor for
224 the virus, hACE2 (*68, 69*). circRNA-encoded SARS-CoV-2 neutralizing nanobodies or hACE2
225 decoy all showed strong neutralizing ability *in vitro*. Given that SARS-CoV-2 variants encoding
226 E484K or N501Y or the K417N-E484K-N501Y evade certain neutralizing antibodies induced by
227 mRNA vaccines (*58, 67*), we anticipated that the effect of circRNA-encoded hACE2 decoy might
228 not be affected by virus mutations.

229 Owing to their specific properties, circRNAs hold potentials in biomedical applications.
230 Nevertheless, the immunogenicity and the safety of circular RNA vaccines or drugs await further
231 investigations.

232

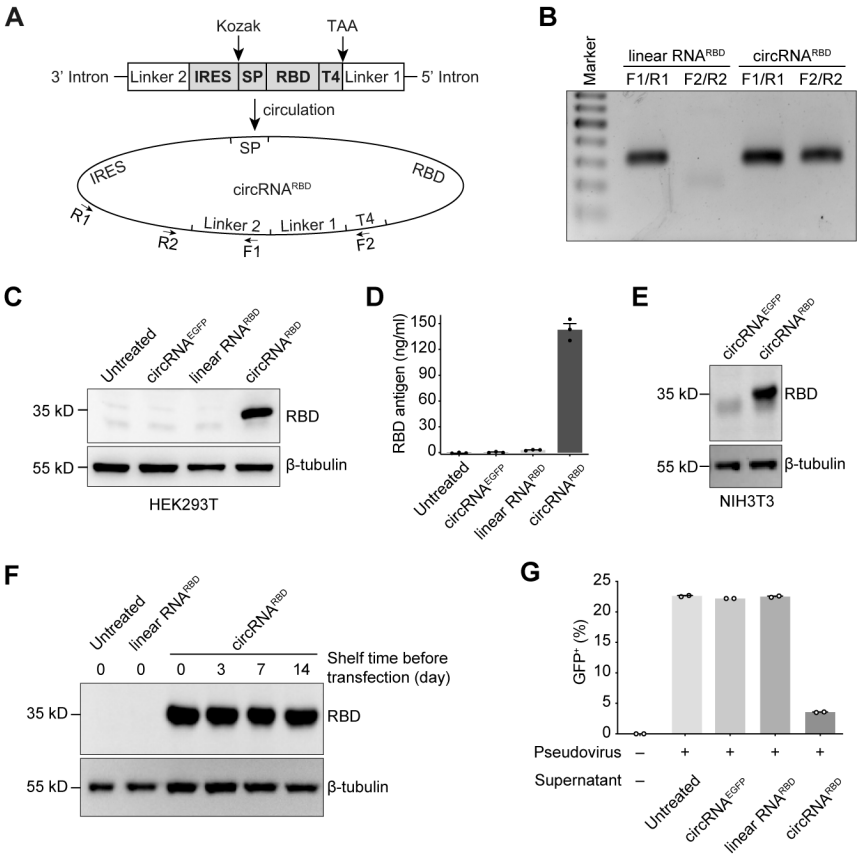

233

234 **Fig. 1. Expression of trimeric SARS-CoV-2 RBD antigens with circular RNAs *in vitro*.** (**A**)
235 Schematic diagram of circRNA^{RBD} circularization by the Group I ribozyme autocatalysis. SP,
236 signal peptide sequence of human tPA protein. T4, the trimerization domain from bacteriophage
237 T4 fibritin protein. RBD, the receptor binding domain of SARS-CoV-2 Spike protein. The arrows
238 indicate the the design of primers for PCR analysis. (**B**) The agarose gel electrophoresis result of
239 the PCR products of linear RNA^{RBD} and circRNA^{RBD}. (**C**) Western Blot analysis showing the
240 expression level of RBD antigens in the supernatant of HEK293T cells transfected with
241 circRNA^{RBD}. The circRNA^{EGFP} and linear RNA^{RBD} were set as controls. (**D**) The quantitative
242 ELISA assay to measure the concentration of RBD antigens in the supernatant. The data in (**B**)
243 was shown as the mean ± S.E.M. (n = 3). (**E**) Western Blot analysis showing the expression level
244 of RBD antigens in the supernatant of mouse NIH3T3 cells transfected with circRNA^{RBD}. The
245 circRNA^{EGFP} was set as controls. (**F**) Western Blot analysis showing the expression level of RBD
246 antigens in the supernatant of HEK293T cells transfected with circRNA^{RBD} for different shelf time
247 (3, 7 or 14 days) at room temperature (~25°C). (**G**) Quantification of the competitive inhibition of
248 SARS-CoV-2 pseudovirus infection (EGFP) by the circRNA^{RBD}-translated RBD antigens. The

249 circRNA^{EGFP} and linear RNA^{RBD} were set as controls. The data in (**E**) was shown as the mean ±
250 S.E.M. (n = 2).

251

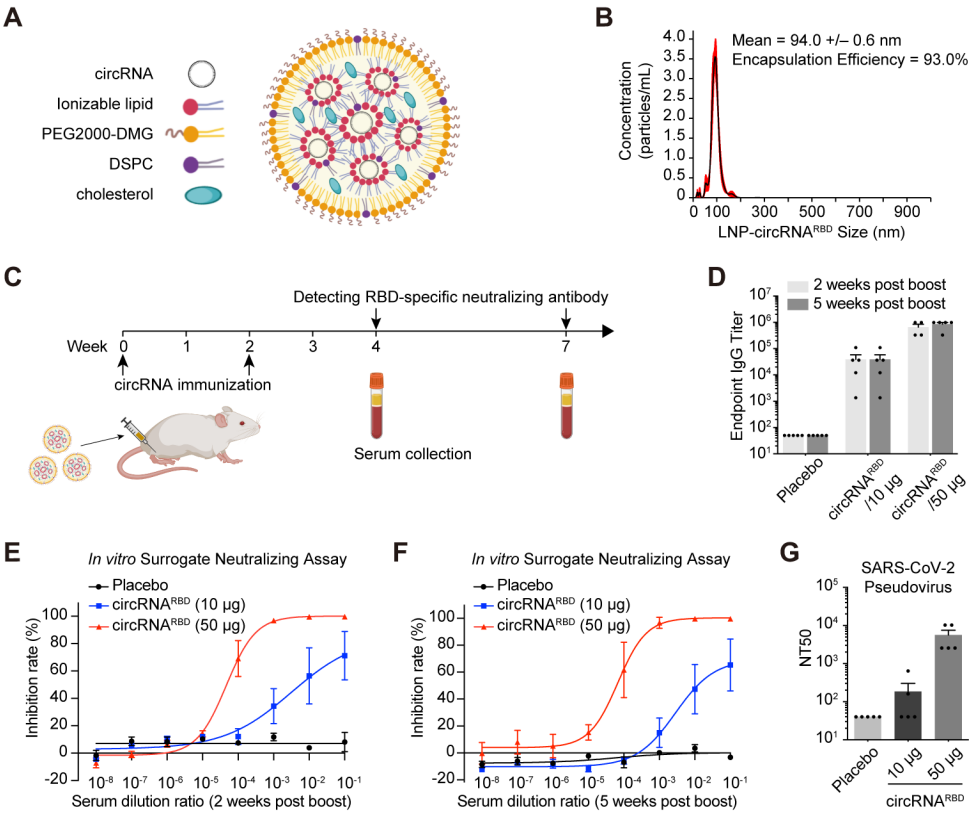

Fig. 2. Humoral immune responses in mice immunized with SARS-CoV-2 circRNA^{RBD} vaccines. (**A**) Schematic representation of LNP-circRNA complex. (**B**) Representative of concentration-size graph of LNP-circRNA^{RBD} measured by dynamic light scattering method. (**C**) Schematic diagram of the LNP-circRNA^{RBD} vaccination process in BALB/c mice and serum collection schedule for specific antibodies analysis. (**D**) Measuring the SARS-CoV-2 specific IgG antibody titer with ELISA. The data were shown as the mean ± S.E.M. (n = 4 or 5). (**E**) Sigmoidal curve diagram of the inhibition rate by sera of immunized mice with surrogate virus neutralization assay. Sera from circRNA^{RBD} (10 μg) and circRNA^{RBD} (50 μg) immunized mice were collected at 2 weeks post the second dose. The data was shown as the mean ± S.E.M. (n = 4). (**F**) Sigmoldal curve diagram of the inhibition rate by sera of immunized mice with surrogate virus neutralization assay. Sera from circRNA^{RBD} (10 μg) and circRNA^{RBD} (50 μg) immunized mice were collected at 5 weeks post boost. The data were shown as the mean ± S.E.M. (n = 5). (**G**) The NT50 was calculated using lentivirus-based SARS-CoV-2 pseudovirus. The data was shown as the mean ± S.E.M. (n = 5).

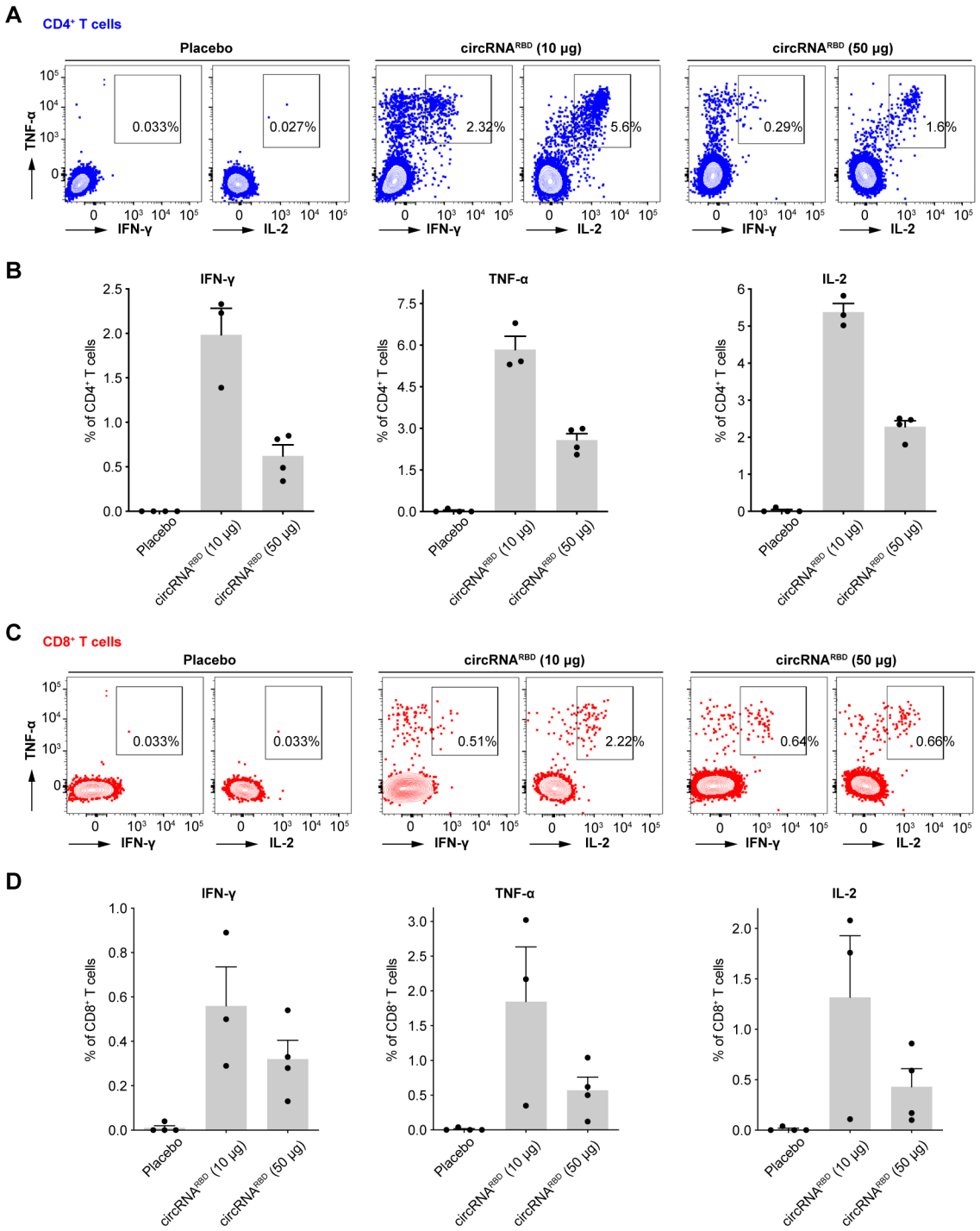

Fig. 3. SARS-CoV-2 specific T cell immune responses in mice immunized with SARS-CoV-2 circRNA^{RBD} vaccines. (**A**) The FACS analysis results showing the percentages of cytokine positive cells evaluated among single and viable CD44^{+}CD62L^{-}CD4^{+} T cells. (**B**) The intracellular staining assay for cytokines (IFN-γ, TNF-α, and IL-2) production among SARS-CoV-2 specific CD4^{+} effector memory T cells (CD44^{+}CD62L^{-}) in splenocytes. (**C**) The FACS analysis results

274 showing the percentages of cytokine positive cells evaluated among single and viable
275 $CD44^{+}CD62L^{-}CD8^{+}$ T. (**D**) The intracellular staining assay for cytokines (IFN-γ, TNF-α, and IL-
276 2) production among SARS-CoV-2 specific $CD8^{+}$ effector memory T cells ($CD44^{+}CD62L^{-}$) in
277 splenocytes. Results were pooled from two independent experiments (**B** and **D**). Data are presented
278 as the mean ± S.E.M. in C and D, n = 3 or 4 for each group. Each symbol represents an individual
279 mouse.

280

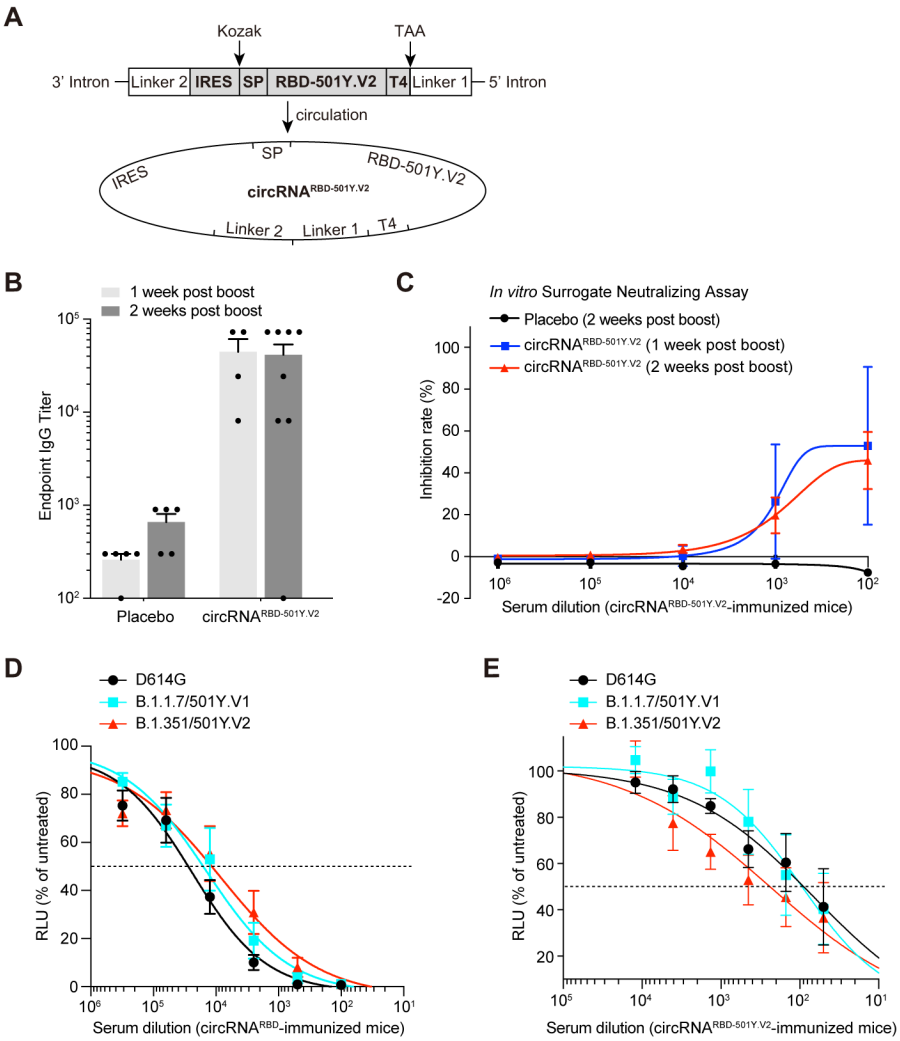

Fig. 4. The susceptibility of SARS-CoV-2 D614G, B.1.1.7 or B.1.351variants to neutralizing antibodies elicited by the circRNA^{RBD} or circRNA$^{RBD\text{-}501Y.V2}$ vaccines in mice. (**A**) Schematic diagram of circRNA$^{RBD\text{-}501Y.V2}$ circularization by the Group I ribozyme autocatalysis. SP, signal peptide sequence of human tPA protein. T4, the trimerization domain from bacteriophage T4 fibritin protein. RBD-501Y.V2, the RBD antigen harboring the K417N-E484K-N501Y mutations in SARS-CoV-2 501Y.V2 variant. (**B**) Measuring the SARS-CoV-2 specific IgG antibody titer with ELISA. The data was shown as the mean ± S.E.M. Each symbol represents an individual mouse. (**C**) Sigmodal curve diagram of the inhibition rate by sera of immunized mice with surrogate virus neutralization assay. Sera from circRNA$^{RBD\text{-}501Y.V2}$ (50 μg) immunized mice were collected at 1 week or 2 weeks post boost. The data were shown as the mean ± S.E.M. (**D**) Neutralization assay of VSV-based D614G, B.1.1.7 or B.1.351 pseudovirus with the serum of mice immunized with circRNA^{RBD} vaccines. The serum samples were collected at 5 weeks post boost. The data were

294 shown as the mean ± S.E.M. (n = 5). (**E**) Neutralization assay of VSV-based D614G, B.1.1.7 or
295 B.1.351 pseudovirus with the serum of mice immunized with circRNA$^{RBD\text{-}501Y.V2}$ vaccines. The
296 serum samples were collected at 1 week post boost. The data were shown as the mean ± S.E.M. (n
297 = 5).

298

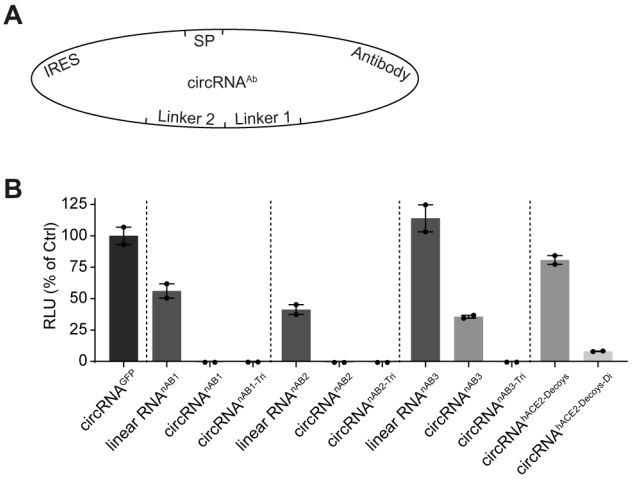

Fig. 5. Expression of SARS-CoV-2 neutralizing nanobodies or hACE2 decoys via circRNA platform. (**A**) Schematic diagram of circRNA^{nAB} or circRNA$^{hACE2\ decoys}$ circularization by the Group I ribozyme autocatalysis. (**B**) Lentivirial-based pseudovirus neutralization assay with the supernatant from cells transfected with circRNA encoding neutralizing nanobodies nAB1, nAB1-Tri, nAB2, nAB2-Tri, nAB3 and nAB3-Tri or ACE2 decoys. The luciferase value was normalized to the circRNA^{EGFP} control. The data was shown as the mean ± S.E.M. (n = 2).

308 **Supplementary Figure Legends**

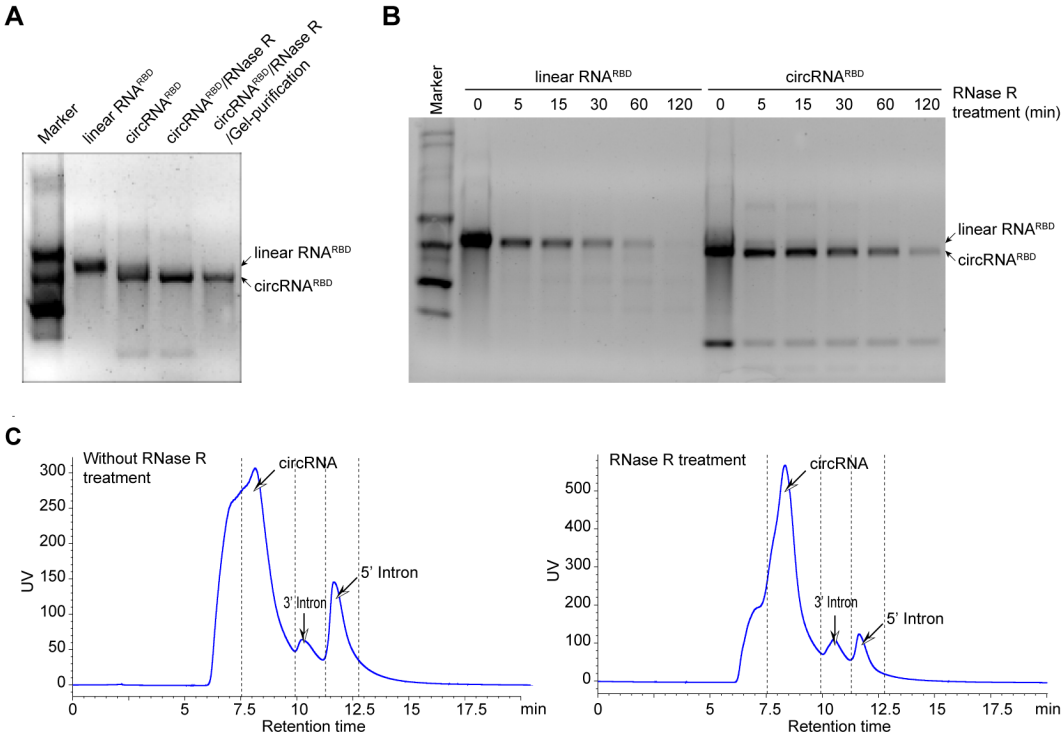

309

310 **fig S1: Agarose gel electrophoresis and HPLC purification of circRNA^{RBD}.** (**A**) The agarose
311 gel electrophoresis result of linear RNA^{RBD} and circRNA^{RBD} with different treatment. (**B**) The
312 agarose gel electrophoresis result of circRNA^{RBD} and linear RNA^{RBD} digested by RNase R with
313 various time from 5 min to 120 min. (**C**) HPLC chromatogram of circRNA^{RBD} without RNase R
314 treatment (left) and circRNA^{RBD} treated by RNase R (right).

315

316

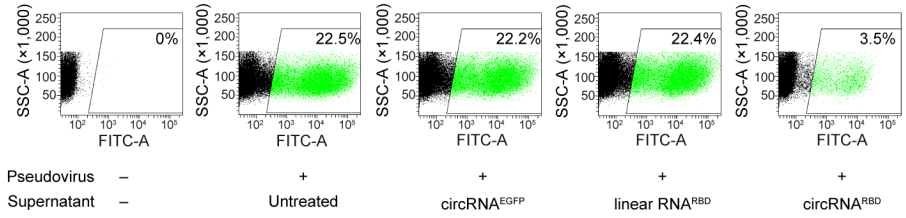

fig S2: The FACS chromatogram of the competitive inhibition of SARS-CoV-2 pseudovirus infection (harboring EGFP reporter) by the circRNA^{RBD}-translated RBD antigens.

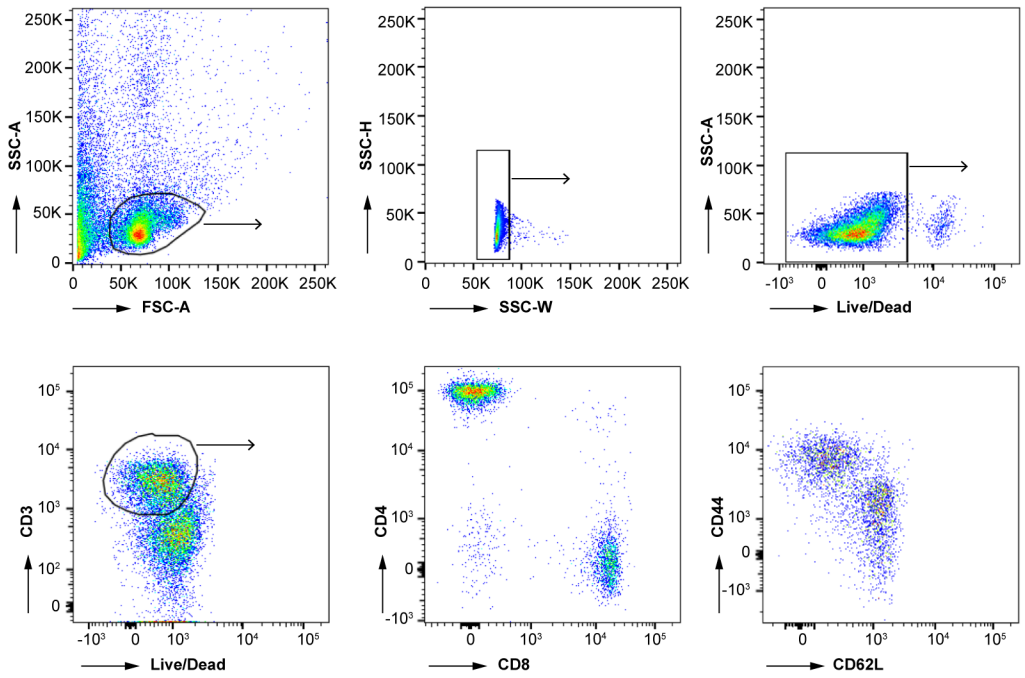

fig S3: Flow panel and gating strategy to quantify SARS-CoV-2-RBD-specific T cells in mice. The plots showed the gating strategy of single and viable T cells from spleens. $CD4^+$ or $CD8^+$ T cells were further analyzed with the expression of CD44 and CD62L.

328

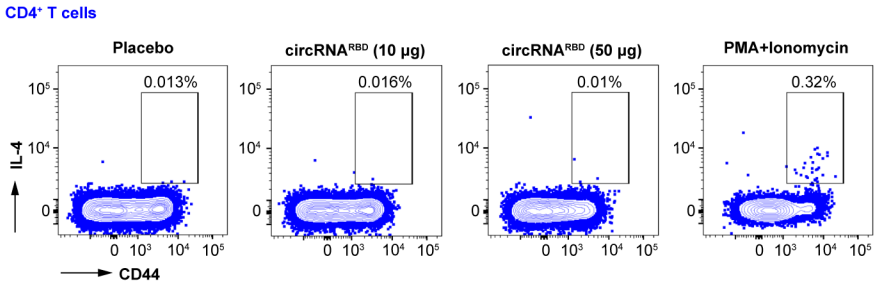

329 **fig S4: Identification of IL-4 producing CD4$^+$ T cells in mice immunized with SARS-CoV-2**
330 **circRNA^{RBD} vaccines.** Splenocytes were stimulated with SARS-CoV-2-RBD peptides for 7 hr in
331 the presence of BFA and Monensin. PMA and Ionomycin stimulation were applied as a positive
332 control. Cells were gated on single and viable CD4$^+$ T cells. The plots are representative for two
333 independent experiments with same results.

334

335

336 **Materials and methods**

337 ***Cell culture***

338 HEK293T and NIH3T3 cell lines were maintained in our laboratory. The HEK293T-hACE2 cell
339 line was ordered from Biodragon Inc. (#BDAA0039, Beijing, China). These mammalian cell lines
340 were cultured in Dulbecco′s Modified Eagle Medium (Corning, 10-013-CV) with 10% fetal bovine
341 serum (FBS) (BI), supplemented with 1% penicillin-streptomycin in 5% CO_2 incubator at 37°C.
342 The Huh-7 cells were maintained in Xie laboratory at Peking University, cultured with the methods
343 previously described (*61*).

344

345 ***circRNA transfection in vitro***

346 For the circRNA transfection in HEK293T or NIH3T3 cells, 3×10^5 cells per well were seeded in
347 12-well plates. 4 μg of RNase R-treated or HPLC-purified & CIP-treated circRNAs were
348 transfected into the HEK293T or NIH3T3 cells, 24 hr later, using Lipofectamine MessengerMax
349 (Invitrogen, LMRNA003) according to the manufacturer's instructions. 48 hr post transfection,
350 the cell lysis and supernatant were collected for the following detections.

351

352 ***LNP encapsulation of circRNA***

353 The circRNAs were encapsulated with lipid nanoparticle (LNP) through a previously described
354 process (*70*). Briefly, the circRNAs were diluted in the 50 mM citrate buffer (pH 3.0) and the lipids
355 were dissolved and mixed in ethanol at molar ratios of 50:10:38.5:1.5 (MC3-
356 lipid:DSPC:cholesterol:PEG2000-DMG). The lipids mixture was then mixed with the circRNA
357 solution at the volume ratio of 1:3 in the NANOASSEMBLR BENCHTOP (PRECISION,
358 #NIT0046). Then the LNP-circRNA formulations were diluted 40-fold with the 1×PBS buffer (pH
359 7.2~7.4) and concentrated by ultrafiltration with Amicon® Ultra Centrifugal Filter Unit
360 (Millipore). The concentration and encapsulation rate of circRNAs were measured by the Quant-
361 iT™ RiboGreen™ RNA Assay Kit (Invitrogen™ #R11490). The size of LNP-circRNA particles
362 was measured using dynamic light scattering on a Malvern Zetasizer Nano-ZS 300 (Malvern).
363 Samples were irradiated with red laser (l = 632.8 nm) and scattered light were detected at a

364 backscattering angle of 173. Results were analyzed to obtain an autocorrelation function using the
365 software (Zetasizer V7.13).

366

367 ***Circulation fragments PCR assay***

368 The circRNA^{RBD} or linear RNA^{RBD} was reverse transcribed into cDNA templates using specific
369 primers with Quantscript RT Kit (KR103, TIANGEN). Then the internal control fragments and
370 junction fragments were PCR amplified from the above cDNA templates with corresponding
371 primers, respectively.

372

373 ***Quantitative determination of SARS-CoV-2 Spike RBD expression in vitro***

374 Quantification of RBD expression in cell culture supernatants was performed with a commercial
375 SARS-CoV-2 Spike RBD Protein ELISA kit (RK04135, ABclonal) according to the
376 manufacturer's instruction. The supernatants were diluted at 1:100 rate. Final concentrations of
377 RBD were calculated basing on the linear standard curve of absorbance at 450 nm, using 630 nm
378 as reference. Briefly, the detection wells were pre-coated with monoclonal antibody specific for
379 Spike RBD protein. After incubation with samples or standards at 37°C for two hours, samples
380 unbound to immobilized antibody would be removed by washing steps. Then the RBD-specific
381 antibodies were added to wells for one-hour incubation at 37°C. After washing, the HRP substrates
382 and stop solution were added and the absorbance at 450 nm were measured using 630 nm as
383 reference.

384

385 ***Mouse vaccination and serum collection***

386 The BALB/c mice were ordered from Beijing Vital River Laboratory Animal Technology Co., Ltd.
387 All mice were bred and kept under SPF (specific pathogen-free) conditions in the Laboratory
388 Animal Center of Peking University. The animal experiments were approved by Peking University
389 Laboratory Animal Center (Beijing), and undertaken in accordance with the National Institute of
390 Health Guide for Care and Use of Laboratory Animals.

391 For mouse vaccination, groups of 6-8 week-old female BLAB/c mice were intramuscularly
392 immunized with LNP-circRNA^{RBD} (10 μg, N = 5; 50 μg, N = 5), or Placebo (empty LNP, N = 5)
393 in 150 μL using a 1 mL sterile syringe, and 2 weeks later a second dose was immunized to boost
394 the immune responses. The sera of immunized mice were collected at 2 and 5 weeks post the
395 second immunization to detect the SARS-CoV-2-specific IgG titers and neutralizing antibody
396 activity as described below. At 5 weeks post the second immunization, the immunized mice were
397 sacrificed and the splenocytes were isolated for the detection of SARS-CoV-2-specific $CD4^+$ and
398 $CD8^+$ T cell immune responses by Flow cytometry analysis and ELISA as described below.

399

400 ***Antibody titer measurement with ELISA***

401 All the immunized mouse serum samples were heat-inactivated at 56°C for 30 min before use. The
402 SARS-CoV-2-specific IgG antibody titer was measured by ELISA. Briefly, serial 3-fold dilutions
403 (in 1% BSA) of heat-inactivated sera, starting at 1:50, were added to the 96-well plates (100
404 μL/well; Costar) coated with recombinant SARS-CoV-2 Spike antigens (Sino Biological) and
405 blocked with 1% BSA, and the plates were incubated for at 37°C for 60 min. Then, after three
406 washes with wash buffer, the Horseradish peroxidase HRP-conjugated rabbit anti-mouse IgG
407 (Sigma) diluted in 1% BSA at 1:10,000 ratio (Sigma), was added to the plates and incubated at
408 37°C for 45 min. Then the plates were washed for 4 times with wash buffer and added with TMB
409 substrates (100 μL/well) followed by incubation for 15-20 min. And then the ELISA stop buffer
410 was added into the plates. Finally, the absorbance (450/630 nm) was measured with Infinite M200
411 (TECAN). The Endpoint IgG titers were defined as the dilution, which emitted an optical density
412 exceeding 3x background (without serum but secondary antibody was added).

413

414 ***SARS-CoV-2 Surrogate Virus Neutralization Assay***

415 The neutralizing activity of mouse serum samples was detected by SARS-CoV-2 Surrogate Virus
416 Neutralization Test Kit (L00847A, GenScript). Detections were performed according to
417 manufacturer's instruction. Serial 10-fold dilutions of heat-inactivated sera, starting at 1:10, were
418 incubated with HRP-conjugated RBD solutions at 37°C for half an hour, and then the mixtures
419 were added into 96-well plates pre-coated with human ACE2 (hACE2) proteins and incubated for

420 15 min at 37°C. After washing the TMB substrates and stop solutions were added and the
421 absorbance (450/630 nm) was measured with Infinite M200 (TECAN). The inhibition rates of
422 serum samples were calculated according to the following formula. The half-neutralization titer of
423 serum (NT50) was determined using four-parameter nonlinear regression in Prism 8 (GraphPad).

424 Inhibition rate = (1- OD value of sample/OD value of negative control) × 100%

425

426 ***Pseudovirus-based neutralization assay***

427 The production of lentivirus-based SARS-CoV-2 pseudovirus and neutralization assay were
428 performed as described previously (*71*). Briefly, the SARS-CoV-2 pseudovirus were produced by
429 co-transfecting plasmids psPAX2 (6 μg), pSpike (6 μg), and pLenti-Luc-GFP (6 μg) into
430 HEK293T cells using X tremeGENE HP DNA Transfection Reagent (Roche) according to the
431 manufacturer′s instructions. 48 hr post transfection, the supernatants containing pseudovirus
432 particles were harvested and filtered through a 0.22-μm sterilized membrane for the neutralization
433 assay as described below.

434 For the determination of NT50 of immunized mouse serum, the HEK293T-hACE2 cells were
435 seeded in 96-well plates (50,000 cells/well) and incubated for approximate 24 hr until reaching
436 over 90% confluent, preparing for pseudovirus infection. The mouse serum was 3-fold diluted,
437 starting at 1:40, and incubated with the SARS-CoV-2 pseudovirus (MOI ≈ 0.05) at 37°C for 60
438 min. The DMEM medium without serum was used as the negative control group. Then the
439 supernatant of HEK293T-hACE2 cells were removed and the mixer of serum and pseudovirus
440 were added to each well. 36-48 hr later, the luciferase activity, which reflecting the degree of
441 SARS-CoV-2 pseudovirus transfection, was measured using the Nano-Glo Luciferase Assay
442 System (Promega). The 50% neutralization titer (NT50) was defined as the fold-dilution, which
443 emitted an exceeding 50% inhibition of pseudovirus infection in comparison with the control group.

444 The neutralization assay of VSV-based pseudovirus of SARS-CoV-2 and variants was performed
445 as described previously (*61, 62*). Briefly, serum was diluted at 1:100 with 5 additional serial 5-
446 fold dilution, and incubated with the same volume of pseudovirus with a $TCID_{50}$ of 1.3×10^4 for 60
447 min at 37°C. 20,000 Huh-7 cells/well were cultured with mixture at 37°C for 24 h. Luciferase
448 activity was measured using the britelite plus Reporter Gene Assay System (PerkinElmer).

449 Relative luciferase units (RLU) were normalized to untreated groups, and analyzed by four-
450 parameter nonlinear regression in Prism (GraphPad).

451 For the neutralization assay of circRNA^{nAB} or circRNA$^{ACE2\ decoys}$, the HEK293T-hACE2 cells
452 were seeded in 96-well plates (50,000 cells/well) and incubated for approximate 24 hr until
453 reaching over 90% confluent. The pseudovirus were pre-incubated with the supernatant of the
454 circRNA^{nAB} or circRNA$^{ACE2\ decoys}$ transfected cells at 37°C for 60 min, and then added to cells in
455 the 96-well plates. Media were changed at 24 hr after transduction. All cells were collected at 48
456 hr after transduction. Luciferase activity was measured using the Nano-Glo Luciferase Assay
457 System (Promega). The relative luminescence units were normalized to cells infected with
458 supernatant of cell transfected with the circRNA^{EGFP}.

459

460 ***T cell flow cytometry analysis***

461 The Splenocytes from each immunized mouse were cultured in R10 media (RPMI 1640
462 supplemented with 1% Pen-Strep antibiotic, 10% HI-FBS), stimulated with RBD peptide pools
463 (Table S1) (Sangon Biotech) for 7 hr at 37°C with protein transport inhibitor cocktail (added 3 hr
464 later). Peptide pools were used at a final concentration of 2 μg/mL for each peptide. Cells from
465 each group were pooled for stimulation with cell stimulation cocktail (PMA/Ionomycin) as a
466 positive control. Following stimulation, cells were washed with PBS prior to staining with
467 LIVE/DEAD for 20 min at room temperature. Cells were then washed in stain buffer (PBS
468 supplemented with 2.5% FBS) and suspended in Fc Block for 5 min at RT prior to staining with a
469 surface stain of following antibodies: CD3 (Invitrogen, 45-0031-82)/CD4 (BD, 562285)/CD8 (BD,
470 553035)/CD69 (BD, 557392)/CD44 (BD, 563058)/CD62L (BD, 560507). After 20 min, cells were
471 washed with stain buffer, and then fixed and permeabilized using the BD Cytoperm
472 fixation/permeabilization solution kit according to manufacturer instructions. Cells were washed
473 in perm/wash solution, followed by intracellular staining (30 min, RT) using a cocktail of the
474 following antibodies: IFN-γ (BD, 557998)/IL-2 (BD, 560547)/IL-4 (BD, 554435)/TNF-a (BD,
475 557644). Finally, cells were washed in perm/wash solution and suspended in stain buffer. Samples
476 were washed and acquired on a LSRFortessa (BD Biosciences). Analysis was performed using
477 FlowJo software.

478

479 ***Expression of neutralizing nanobodies or ACE2 decoys by circular RNAs***

480 HEK293T cells were transfected with circular RNA in transfection reagent. Circular RNA
481 encoding secretary nanobodies or hACE2 decoys were purified after GTP treatment for cyclization.
482 In brief, HEK293T cells were seeded in 12-well plates. After 24 h, cells were transfected with
483 circRNA (4 μg per well) and continuously added fresh medium to a final volume of about 1 ml.
484 Supernatants were harvested at 48 hr post transfection and centrifuged to remove cells.

485

486 **REFERENCES**

487 1. F. Wu *et al.*, A new coronavirus associated with human respiratory disease in China. *Nature* **579**, 265-269
488 (2020).
489 2. P. Zhou *et al.*, A pneumonia outbreak associated with a new coronavirus of probable bat origin. *Nature*
490 **579**, 270-273 (2020).
491 3. P. V'Kovski, A. Kratzel, S. Steiner, H. Stalder, V. Thiel, Coronavirus biology and replication: implications
492 for SARS-CoV-2. *Nat Rev Microbiol* **19**, 155-170 (2021).
493 4. D. Kim *et al.*, The Architecture of SARS-CoV-2 Transcriptome. *Cell* **181**, 914-921 e910 (2020).
494 5. M. Hoffmann *et al.*, SARS-CoV-2 Cell Entry Depends on ACE2 and TMPRSS2 and Is Blocked by a
495 Clinically Proven Protease Inhibitor. *Cell* **181**, 271-280 e278 (2020).
496 6. R. Yan *et al.*, Structural basis for the recognition of SARS-CoV-2 by full-length human ACE2. *Science*
497 **367**, 1444-1448 (2020).
498 7. D. Wrapp *et al.*, Cryo-EM structure of the 2019-nCoV spike in the prefusion conformation. *Science* **367**,
499 1260-1263 (2020).
500 8. J. Shang *et al.*, Cell entry mechanisms of SARS-CoV-2. *Proc Natl Acad Sci U S A* **117**, 11727-11734
501 (2020).
502 9. A. C. Walls *et al.*, Structure, Function, and Antigenicity of the SARS-CoV-2 Spike Glycoprotein. *Cell* **181**,
503 281-292 e286 (2020).
504 10. C. L. Hsieh *et al.*, Structure-based design of prefusion-stabilized SARS-CoV-2 spikes. *Science* **369**, 1501-
505 1505 (2020).
506 11. S. Bangaru *et al.*, Structural analysis of full-length SARS-CoV-2 spike protein from an advanced vaccine
507 candidate. *Science* **370**, 1089-1094 (2020).
508 12. F. Krammer, SARS-CoV-2 vaccines in development. *Nature* **586**, 516-527 (2020).
509 13. A. Mullard, COVID-19 vaccine development pipeline gears up. *Lancet* **395**, 1751-1752 (2020).
510 14. Q. Gao *et al.*, Development of an inactivated vaccine candidate for SARS-CoV-2. *Science* **369**, 77-81
511 (2020).

512 15. N. van Doremalen *et al.*, ChAdOx1 nCoV-19 vaccine prevents SARS-CoV-2 pneumonia in rhesus
513 macaques. *Nature* **586**, 578-582 (2020).
514 16. L. Sanchez-Felipe *et al.*, A single-dose live-attenuated YF17D-vectored SARS-CoV-2 vaccine candidate.
515 *Nature* **590**, 320-325 (2021).
516 17. F. C. Zhu *et al.*, Safety, tolerability, and immunogenicity of a recombinant adenovirus type-5 vectored
517 COVID-19 vaccine: a dose-escalation, open-label, non-randomised, first-in-human trial. *Lancet* **395**, 1845-1854
518 (2020).
519 18. J. Yang *et al.*, A vaccine targeting the RBD of the S protein of SARS-CoV-2 induces protective immunity.
520 *Nature* **586**, 572-577 (2020).
521 19. L. Dai *et al.*, A Universal Design of Betacoronavirus Vaccines against COVID-19, MERS, and SARS. *Cell*
522 **182**, 722-733 e711 (2020).
523 20. J. Yu *et al.*, DNA vaccine protection against SARS-CoV-2 in rhesus macaques. *Science* **369**, 806-811
524 (2020).
525 21. K. S. Corbett *et al.*, SARS-CoV-2 mRNA vaccine design enabled by prototype pathogen preparedness.
526 *Nature* **586**, 567-571 (2020).
527 22. K. S. Corbett *et al.*, Evaluation of the mRNA-1273 Vaccine against SARS-CoV-2 in Nonhuman Primates.
528 *The New England journal of medicine* **383**, 1544-1555 (2020).
529 23. N. N. Zhang *et al.*, A Thermostable mRNA Vaccine against COVID-19. *Cell* **182**, 1271-1283 e1216
530 (2020).
531 24. D. Laczko *et al.*, A Single Immunization with Nucleoside-Modified mRNA Vaccines Elicits Strong
532 Cellular and Humoral Immune Responses against SARS-CoV-2 in Mice. *Immunity* **53**, 724-732 e727 (2020).
533 25. Q. Huang *et al.*, A single-dose mRNA vaccine provides a long-term protection for hACE2 transgenic mice
534 from SARS-CoV-2. *Nature communications* **12**, 776 (2021).
535 26. U. Sahin *et al.*, COVID-19 vaccine BNT162b1 elicits human antibody and TH1 T cell responses. *Nature*
536 **586**, 594-599 (2020).
537 27. A. B. Vogel *et al.*, BNT162b vaccines protect rhesus macaques from SARS-CoV-2. *Nature*, (2021).
538 28. N. Pardi, M. J. Hogan, F. W. Porter, D. Weissman, mRNA vaccines - a new era in vaccinology. *Nat Rev*
539 *Drug Discov* **17**, 261-279 (2018).
540 29. N. A. C. Jackson, K. E. Kester, D. Casimiro, S. Gurunathan, F. DeRosa, The promise of mRNA vaccines: a
541 biotech and industrial perspective. *NPJ Vaccines* **5**, 11 (2020).
542 30. M. Durymanov, J. Reineke, Non-viral Delivery of Nucleic Acids: Insight Into Mechanisms of Overcoming
543 Intracellular Barriers. *Front Pharmacol* **9**, 971 (2018).
544 31. O. S. Fenton *et al.*, Bioinspired Alkenyl Amino Alcohol Ionizable Lipid Materials for Highly Potent In
545 Vivo mRNA Delivery. *Adv Mater* **28**, 2939-2943 (2016).
546 32. R. A. Wesselhoeft *et al.*, RNA Circularization Diminishes Immunogenicity and Can Extend Translation
547 Duration In Vivo. *Mol Cell* **74**, 508-520 e504 (2019).

548 33. Y. G. Chen *et al.*, N6-Methyladenosine Modification Controls Circular RNA Immunity. *Mol Cell* **76**, 96-
549 109 e109 (2019).
550 34. X. O. Zhang *et al.*, Complementary sequence-mediated exon circularization. *Cell* **159**, 134-147 (2014).
551 35. L. L. Chen, The biogenesis and emerging roles of circular RNAs. *Nat Rev Mol Cell Biol* **17**, 205-211
552 (2016).
553 36. L. S. Kristensen *et al.*, The biogenesis, biology and characterization of circular RNAs. *Nat Rev Genet* **20**,
554 675-691 (2019).
555 37. S. Memczak *et al.*, Circular RNAs are a large class of animal RNAs with regulatory potency. *Nature* **495**,
556 333-338 (2013).
557 38. Y. Enuka *et al.*, Circular RNAs are long-lived and display only minimal early alterations in response to a
558 growth factor. *Nucleic Acids Res* **44**, 1370-1383 (2016).
559 39. I. Legnini *et al.*, Circ-ZNF609 Is a Circular RNA that Can Be Translated and Functions in Myogenesis.
560 *Mol Cell* **66**, 22-37 e29 (2017).
561 40. M. Zhang *et al.*, A novel protein encoded by the circular form of the SHPRH gene suppresses glioma
562 tumorigenesis. *Oncogene* **37**, 1805-1814 (2018).
563 41. M. Zhang *et al.*, A peptide encoded by circular form of LINC-PINT suppresses oncogenic transcriptional
564 elongation in glioblastoma. *Nat Commun* **9**, 4475 (2018).
565 42. X. Gao *et al.*, Circular RNA-encoded oncogenic E-cadherin variant promotes glioblastoma tumorigenicity
566 through activation of EGFR-STAT3 signalling. *Nat Cell Biol*, (2021).
567 43. R. A. Wesselhoeft, P. S. Kowalski, D. G. Anderson, Engineering circular RNA for potent and stable
568 translation in eukaryotic cells. *Nat Commun* **9**, 2629 (2018).
569 44. Y. Yang *et al.*, Extensive translation of circular RNAs driven by N(6)-methyladenosine. *Cell Res* **27**, 626-
570 641 (2017).
571 45. Y. Kou *et al.*, Tissue plasminogen activator (tPA) signal sequence enhances immunogenicity of MVA-
572 based vaccine against tuberculosis. *Immunol Lett* **190**, 51-57 (2017).
573 46. J. M. Richner *et al.*, Modified mRNA Vaccines Protect against Zika Virus Infection. *Cell* **169**, 176 (2017).
574 47. N. Pardi *et al.*, Zika virus protection by a single low-dose nucleoside-modified mRNA vaccination. *Nature*
575 **543**, 248-251 (2017).
576 48. K. Papanikolopoulou, M. J. van Raaij, A. Mitraki, Creation of hybrid nanorods from sequences of natural
577 trimeric fibrous proteins using the fibritin trimerization motif. *Methods Mol Biol* **474**, 15-33 (2008).
578 49. K. M. Bouwman *et al.*, Multimerization- and glycosylation-dependent receptor binding of SARS-CoV-2
579 spike proteins. *PLoS Pathog* **17**, e1009282 (2021).
580 50. J. W. Fischer, A. K. Leung, CircRNAs: a regulator of cellular stress. *Crit Rev Biochem Mol Biol* **52**, 220-
581 233 (2017).
582 51. X. Ou *et al.*, Characterization of spike glycoprotein of SARS-CoV-2 on virus entry and its immune cross-
583 reactivity with SARS-CoV. *Nature communications* **11**, 1620 (2020).

584 52. C. W. Tan *et al.*, A SARS-CoV-2 surrogate virus neutralization test based on antibody-mediated blockage
585 of ACE2-spike protein-protein interaction. *Nat Biotechnol* **38**, 1073-1078 (2020).
586 53. A. Sette, S. Crotty, Adaptive immunity to SARS-CoV-2 and COVID-19. *Cell* **184**, 861-880 (2021).
587 54. Y. Xiang *et al.*, Versatile and multivalent nanobodies efficiently neutralize SARS-CoV-2. *Science* **370**,
588 1479-1484 (2020).
589 55. M. Schoof *et al.*, An ultrapotent synthetic nanobody neutralizes SARS-CoV-2 by stabilizing inactive Spike.
590 *Science* **370**, 1473-1479 (2020).
591 56. T. W. Linsky *et al.*, De novo design of potent and resilient hACE2 decoys to neutralize SARS-CoV-2.
592 *Science* **370**, 1208-1214 (2020).
593 57. A. Muik *et al.*, Neutralization of SARS-CoV-2 lineage B.1.1.7 pseudovirus by BNT162b2 vaccine-elicited
594 human sera. *Science*, (2021).
595 58. Z. Wang *et al.*, mRNA vaccine-elicited antibodies to SARS-CoV-2 and circulating variants. *Nature*,
596 (2021).
597 59. P. Wang *et al.*, Antibody Resistance of SARS-CoV-2 Variants B.1.351 and B.1.1.7. *Nature*, (2021).
598 60. W. Tai *et al.*, A novel receptor-binding domain (RBD)-based mRNA vaccine against SARS-CoV-2. *Cell*
599 *Res* **30**, 932-935 (2020).
600 61. Y. Cao *et al.*, Potent Neutralizing Antibodies against SARS-CoV-2 Identified by High-Throughput Single-
601 Cell Sequencing of Convalescent Patients' B Cells. *Cell* **182**, 73-84 e16 (2020).
602 62. S. Du *et al.*, Structurally Resolved SARS-CoV-2 Antibody Shows High Efficacy in Severely Infected
603 Hamsters and Provides a Potent Cocktail Pairing Strategy. *Cell* **183**, 1013-1023 e1013 (2020).
604 63. C. O. Barnes *et al.*, SARS-CoV-2 neutralizing antibody structures inform therapeutic strategies. *Nature*
605 **588**, 682-687 (2020).
606 64. P. A. Koenig *et al.*, Structure-guided multivalent nanobodies block SARS-CoV-2 infection and suppress
607 mutational escape. *Science* **371**, (2021).
608 65. N. G. Davies *et al.*, Increased hazard of death in community-tested cases of SARS-CoV-2 Variant of
609 Concern 202012/01. *medRxiv*, (2021).
610 66. A. S. Lauring, E. B. Hodcroft, Genetic Variants of SARS-CoV-2-What Do They Mean? *JAMA* **325**, 529-
611 531 (2021).
612 67. C. K. Wibmer *et al.*, SARS-CoV-2 501Y.V2 escapes neutralization by South African COVID-19 donor
613 plasma. *Nat Med*, (2021).
614 68. K. K. Chan *et al.*, Engineering human ACE2 to optimize binding to the spike protein of SARS coronavirus
615 2. *Science* **369**, 1261-1265 (2020).
616 69. A. Glasgow *et al.*, Engineered ACE2 receptor traps potently neutralize SARS-CoV-2. *Proc Natl Acad Sci*
617 *U S A* **117**, 28046-28055 (2020).
618 70. L. M. Ickenstein, P. Garidel, Lipid-based nanoparticle formulations for small molecules and RNA drugs.
619 *Expert Opin Drug Deliv* **16**, 1205-1226 (2019).

71. D. Pinto *et al.*, Cross-neutralization of SARS-CoV-2 by a human monoclonal SARS-CoV antibody. *Nature* **583**, 290-295 (2020).

ACKNOWLEDGEMENTS

We acknowledge C. Dong and X. Wang (Tsinghua University) for providing fluorescent-conjugated antibodies. We thank J. Xiao (Peking University) for providing purified SARS-CoV-2 Spike proteins. We thank J. Yan (Institute of Microbiology, Chinese Academy of Sciences) for providing RBD peptide pools. We thank the Laboratory Animal Centre of Peking University for the feeding of mice. We thank the HPLC Core at the National Center for Protein Sciences at Peking University (Beijing), particularly H. Li and G. Li for technical help. We thank the flow cytometry Core at the National Center for Protein Sciences at Peking University (Beijing), particularly H. Lv, Y. Guo, H. Yang, F. Wang for technical help.

Funding:

This project was supported by funds from National Key R&D Program of China (2020YFA0707800 to W.W., 2020YFA0707600 to Z.Z.); Beijing Municipal Science & Technology Commission (Z181100001318009); the National Science Foundation of China (31930016); Beijing Advanced Innovation Center for Genomics at Peking University and the Peking-Tsinghua Center for Life Sciences (to W.W.); the National Science Foundation of China (31870893); the National Major Science & Technology Project for Control and Prevention of Major Infectious Diseases in China (2018ZX10301401 to Z.Z.) and the Fellowship of China National Postdoctoral Program for Innovative Talents (BX20200010, to L.Q.).

Author Contributions:

W.W. conceived and supervised this project. W.W., L.Q. and Z.Y. designed the experiments. L.Q., Z.Y., Y.S., Y.X., Z.W., H.T., A.Y., and X.X. performed the experiments with the help from Z.Z., Y.C., J.W., and X.S.X.. L.Q., Z.Y. and W.W. wrote the manuscript with the help of all other authors.